

## The Isaac Newton Telescope Monitoring Project: Stellar Population in the IC 10 Dwarf Irregular Galaxy

Mahtab Gholami, Mohammad Taghi Mirtorabi

Department of Physics, Alzahra University, Tehran, P.O.Box 1993891176, Iran  
[m.gholami@alzahra.ac.ir](mailto:m.gholami@alzahra.ac.ir); [torabi@alzahra.ac.ir](mailto:torabi@alzahra.ac.ir)

**Abstract.** We have conducted an optical monitoring survey of IC 10 dwarf irregular galaxy in the Local Group, using the *Isaac Newton Telescope* (INT) with the wide-field camera (WFC), to identify the Asymptotic Giant Branch stars (AGBs). AGBs are at the final stage of their evolution and can be implemented as powerful tools for finding the star formation history and chemical evolution of galaxies. The stellar populations in IC 10 had not been previously identified in optical wavebands surveys. Our data set was obtained in the *i*- and *V* - band with the WFC instrument. Photometry was obtained for 48578 stars within the area of  $0.07 \text{ deg}^2$  ( $13.5 \text{ kpc}^2$ ), of which 10800 stars are detected as AGBs. Radial distribution histogram has been constructed in the image plane for populations of AGBs, RGBs (Red Giant Branch stars) and massive stars. We found that the RGBs population has the largest effective radius among the three populations in the IC 10 image plane. Our data were matched to optical catalogues of *Pan-STARRS* (The *Pan-STARRS* release 1 (PS1) survey-DR1) catalogue, mid-infrared catalogue of good sources (DUSTiNGS Good Source Catalog (GSC)) from the *Spitzer Space Telescope* and near-IR catalogue of *Hubble Space Telescope* (*HST*). The number of 441 and 1927 were identified as C-type (carbon-rich) and M-type (oxygen-rich) stars respectively; using the matched stars between our catalogue and the *HST* catalogue.

*Keywords:* Stars: AGB, RSG, RGB, galaxies: Irregular, dwarf

## 1 Introduction

Amongst the dwarf galaxies in the Local Group, the isolated irregular one, IC 10 (UGC 192) is the only dwarf galaxy under violent starbursting phase in the Local Group. Undergoing a starbursting phase, having numerous *HII* regions and being bright in all wavebands, makes it an exquisite galaxy to study. IC 10 is known as a starburst galaxy with a metallicity of ( $[Fe/H] = -1.28 \text{ dex}$ ) [5] and is identified as one of the most massive and luminous galaxies [58] with the high density of Wolf-Rayet stars [9] and classified as the fifth in luminosity in the Local Group. The observations of IC 10 confirmed that central galactic regions contain huge amounts of bright young stars [32]. The existence of a hydrogen cloud around the galaxy had been first discovered by Roberts et al. [45] with observations of neutral hydrogen (HI) which showed the star-forming activities in IC 10. Wilcots et al. [62] found that the structure of hydrogen clouds of IC 10 contain shells and holes produced by stellar winds from bright Wolf-Rayet and Oxygen-rich stars. IC 10 is located within the boundaries of the northern constellation Cassiopeia at ( $l = 118^\circ.9$ ,  $b = -3^\circ.3$ ) [20] with radial velocity of  $V_r = -348 \pm 1 \text{ kms}^{-1}$  [2] and proper motions of  $(-122 \pm 31, 97 \pm 27) \text{ kms}^{-1}$  in *RA* and *DEC* [7]. It is more similar to the Large Magellanic Clouds (*LMC*) observed in the

southern hemisphere. The light of the galaxy is affected by gas-dust clouds of Milky Way because of locating in the Milky Way zone ( $b = -3.^\circ 3$ ) [59]. Therefore, studying IC 10 is restricted due to the strong extinction of our galaxy. Several studies have been performed to determine the real distance to IC 10. Massey et al. [40] obtained the distance of about 1 Mpc by identifying a blue plume of the main-sequence luminous stars in the  $B$  versus  $(B - V)$  Colour-Magnitude Diagram (CMD). Borissova et al. [3] obtained the distance of  $m - M = 23.86 \text{ mag}$  by comparison between the supergiants of IC 10 and those of IC 1613 dwarf galaxy. Demers et al. [11] calculated the reddening and distance using 676 carbon stars and obtained the distance to the galaxy as  $741 \pm 37 \text{ kpc}$ . Kim et al. [33] estimated the distance to the IC 10 of  $715 \pm 10 \text{ kpc}$  and Lim et al. and Leroy et al. [37, 34] obtained the distance of 700 kpc and Sanna et al. estimated the distance modulus of  $m - M = (23.51 \pm 0.15 \text{ mag})$ , corresponding to the distance of 715 kpc [47, 48]. In this study, we use the distance modulus which is estimated by McConnachie12 [41] of  $m - M = (24.27 \pm 0.18 \text{ mag})$ , corresponding to the distance of  $794 \pm 44 \text{ kpc}$ .

Asymptotic giant branch stars (AGBs) and red supergiant stars (RSGs) are identified as the last phase of post-main sequence stellar evolution. AGBs are evolved stars with intermediate mass of  $1 M_\odot \lesssim M \lesssim 8 M_\odot$  that are identified by periods of mass loss. They show variability in magnitude which their amplitudes and periods increase as the star evolves [15, 63]. Dust production from mass-loss in AGBs increases at the final stage of their evolution and these stars can be recognized with their longest periods and largest amplitudes [61, 38, 21, 24, 42]. McQuinn et al. [42] classified AGBs to two basic phases: (1) E-AGBs (Early-AGBs) phase which are identified by shell He-burning and (2) AGB-tip (thermally-pulsating AGB) phase which are characterized when shell He-burning tends to run out of fuel. Most of the AGBs are distinguishable as Long-Period Variables (*LPVs*) due to the strong thermal radial pulsations of their cool atmospheric shells with the period of few tens of days to more than 1000 days [22].

Unlike the Sloan et al. [53, 54] and Boyer et al. [4] that explained the weak dependency of C-type (carbon-rich) stars in metallicity, van Loon et al. [60] showed the significant metallicity dependency in Carbon-rich AGBs. The dusty Oxygen-rich stars are more important at early times because the most massive AGBs are oxygen rich M-type stars [6, 3]. Star formation history (SFH) and chemical environment are the two most important factors to characterizing the dwarf galaxies [44]. The existence of large amounts of bright young stars and extended *HII* regions of IC 10 reveal the high star-forming activity. IC 10 is a starburst galaxy contains huge amounts of carbon dust which produced by AGBs [10]. This study is a part of an ongoing project of optical monitoring survey of dwarf galaxies in the Local Group, using INT for three years [49, 50, 51, 17, 14]. Our aim is identifying the Long-period variable stars (LPVs) for these galaxies. We will use the mass function of LPVs to define the star formation history [14, 16, 17, 19, 18, 23, 24, 30, 50, 51, 52]. AGBs and RSGs with radial pulsation at their atmospheric layers are identified as LPVs with the brightness variation time of the order of 150-1500 days in their photometric light curves [25]. In this paper, we aim to investigate the stellar population in the IC 10 galaxy. Our next papers will cover identifying the LPVs, star formation history and dust production at this galaxy. We classified this paper as follows; Details of the observational data are described in section 2. In section 3, the method of photometry is presented and we summarize and discuss our conclusions in section 5 and 6.

Table 1: Log of WFC observations of IC 10 dwarf galaxy.

Date (y m d)	Filter	Epoch	Exposure time (sec)	Airmass	Seeing (arcsec)
2016 06 15	i	1	555	2.271	1.82
2016 08 10	i	2	555	1.168	1.11
2016 08 13	V	1	735	1.331	1.69
2016 10 19	i	3	555	1.303	1.55
2016 10 19	V	2	735	1.361	1.62
2017 08 01	i	4	555	1.496	1.35
2017 08 01	V	3	735	1.411	1.40
2017 09 01	i	5	555	1.263	1.47
2017 09 01	V	4	735	1.225	1.62
2017 09 02	i	6	555	1.634	1.18
2017 09 02	V	5	735	1.525	1.43
2017 10 06	i	7	555	1.263	1.24
2017 10 08	V	6	735	1.184	1.11

## 2 Observation

We have conducted an optical monitoring survey of the majority of dwarf galaxies in the Local Group, with the Isaac Newton Telescope (INT) for three years [14, 17, 22, 25, 26, 28, 30, 44, 49, 51]. The IC 10 galaxy was observed in 9 nights dated from June, 2016 to October, 2017, using the Wide Field Camera (WFC). The maximum value of seeing parameter was not greater than 1.82 arcsec that corresponds to high airmass of 2.271 (zenith angle  $\sim 63^\circ$ ). The WFC is an optical mosaic camera at the 2.5 m Isaac Newton Telescope (INT) of the *Observatorio del Roque de Los Muchachos (La Palma)*. It contains four 2048 x 4096 CCDs with a pixel size of 0.33 arcsec/pixel. We used Transforming HEavenly Light into Image (THELI) for the automated pre-reduction of astronomical images [12]. Observations were performed in Sloan *i* and Harris *V* filters. We selected *i* – *band* images as AGBs identifier because of the peak of Spectral Energy Distribution (SED) of AGBs is located around  $1\mu\text{m}$  [28, 29]. The observational log which contains exposure time, airmass and seeing is listed in table 1.

## 3 Photometry

The photometry process for the IC 10 as a crowded stellar field carried out using the Stetson package [55, 57, 56] by fitting Point-Spread Function (PSF) on selected individual stars on each image separately then implementing PSF photometry to determine *i* – *band* and *V* – *band* magnitudes. A number of 20-50 PSF models were produced depending on crowdedness of image. To ensure that the PSF models are adequate for the entire image we subtracted observed image from synthetic image using appropriate PSF for each star and found no residual error more than observed noise level. We used DAOMATCH routine to find rough coordinate transformations between the images. Then, we used DAOMASTER routine to refine the transformations generated by DAOMATCH.

The MONTAGE routine was executed to combine the individual images in both *i* and *V* filters to create the median image and subtract off an approximate sky value from each frame. The median image of IC 10 is shown in Fig. 1. A master list of stars was produced

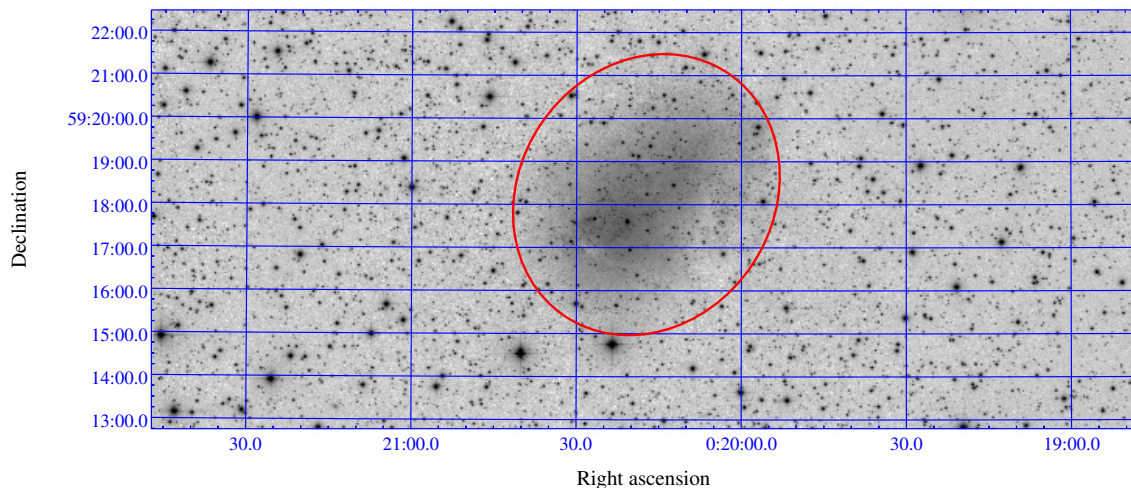


Figure 1: Median  $i$ -band mosaic image of the IC 10 dwarf galaxy. The red ellipse is marked as the half-light radius of the galaxy.

using ALLFRAME routine which implements PSF photometry. Because of the differences in full width at half maximum (FWHM) in each image we used PSF created for each image separately. We obtained the residual magnitude between the PSF fitted values and magnitudes taken from largest aperture photometry using DAOGROW routine. We created the growth-curves for all subtracted stars except of the PSF stars at each frame. The growth-curve analysis is needed to improve the accuracy of the total flux measurement with measuring the magnitude of the bright and isolated stars in each frame through a series of several concentric apertures of increasing radius. The observed magnitude differences between successive apertures were calculated for each star [56]. Then, The differences between the PSF-fitting photometry model magnitude and the one in the largest aperture photometry were obtained by COLLECT routine, to measure aperture correction. CCDAVE routine was applied to calibrating the stars at the master list. Finally, the NEWTRIAL routine was performed to calculate and apply the aperture corrections, convert instrumental magnitudes to the standard system, and find the weighted mean magnitude for stars in all frames.

We obtained the zero-points for each frame to calibrate all the frames based on the measurement of the standard stars. The accurate zero-points were measured by transformation equations [31]. We used the average of zero-points for the nights without standard stars observations. Accurate extinction determination has an important impact in extracting the parameters of the galaxy [59]. The Airmass-dependent atmospheric extinction was applied by adopting the extinction coefficients of  $0.0197 \text{ mag}$  and  $0.1036 \text{ mag}$  in  $i$ - and  $V$ -band, respectively which were determined for *LA Palma* [13]. In addition to the atmospheric extinction, we considered the extinctions caused by Milky Way and IC 10 which is measured using two components: The external component which produced by the gas or dust clouds of Milky Way and internal extinction inside of the IC 10. The clouds of dust and gas which are observed in the images of IC 10 show the absorption and scattering of light in the galaxy which confirm the existence of extinction inside of the galaxy. Generally, the combination of these two components led to obtaining the combined extinction for the galaxy [59]. Comparison of the Atmospheric extinction with the combined extinction (external and internal extinction components) confirmed that the combined extinction is a major factor to deter-

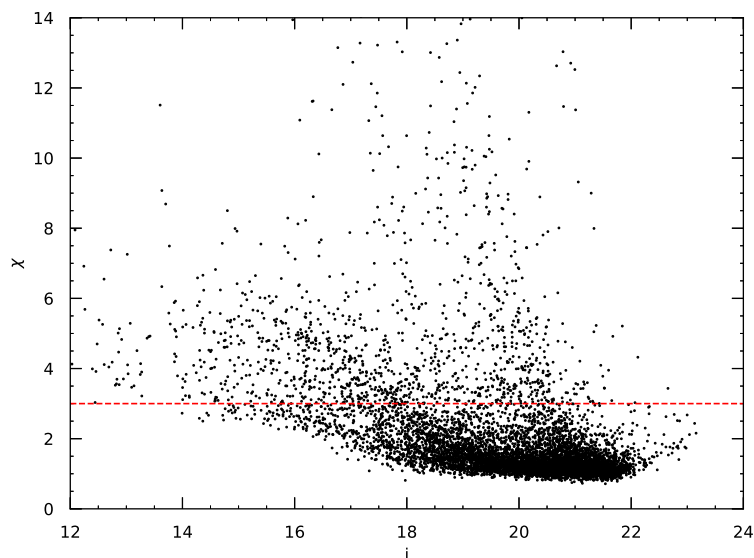


Figure 2: The  $\chi$  values versus  $i$  – *band* magnitude for stars in one of the individual frames. The red dashed line shows the  $\chi$  criterion.

mine the physical parameters for this galaxy.

The  $\chi$  value is defined for each star as a robust estimate of the ratio of the observed pixel-to-pixel scatter from the radial profile of the image divided by the expected pixel-to-pixel scatter from the image profile. Furthermore, The sharpness value is also defined as the ratio of the bivariate delta-function which best fits the brightness peak in the original image to the height of the bivariate Gaussian function (with the user-supplied value of the FWHM) which best fits the peak. We assumed a cut off on the  $\chi$  value for each frame based on the  $\chi$  values distribution of all stellar objects which have  $\chi < 3$ . Thus, the non-stellar objects have been removed from our catalogue if they considered at the  $\chi$  criterion. Fig. 2 shows the  $\chi$  value of stars versus  $i$  – *band* magnitude for one of the individual frames. The horizontal red dashed line shows the selection criteria of  $\chi < 3$ . Fig. 3 shows the sharpness value of stars versus  $i$  – *band* magnitude for one of the individual frames. The sharpness values for all sources are shown with black dots and the sharpness values for stars with the  $\chi < 3$  criteria are shown with red dots.

To increase accuracy in magnitude measurements, we calibrated the images relative to each other. The relative calibration has been carried out by a selection of approximately 800 stars in common between all images with the magnitudes of  $18 \leq i \leq 22 \text{ mag}$ . These selected stars were averaged in magnitude for each image and then photometry was complemented by applying the corrections between  $-0.000925$  and  $0.00751 \text{ mag}$  that equalized these mean magnitudes against each other. The relative calibration corrections added to the magnitudes in each of individual images and then the averaged values have been calculated again for the selected stars of each image. Fig. 4 shows the correction as a function of time for all of the images before applying the correction values. As can be seen, the corrections are less than 1 per cent which shows that the images are satisfactory calibrated to each other.

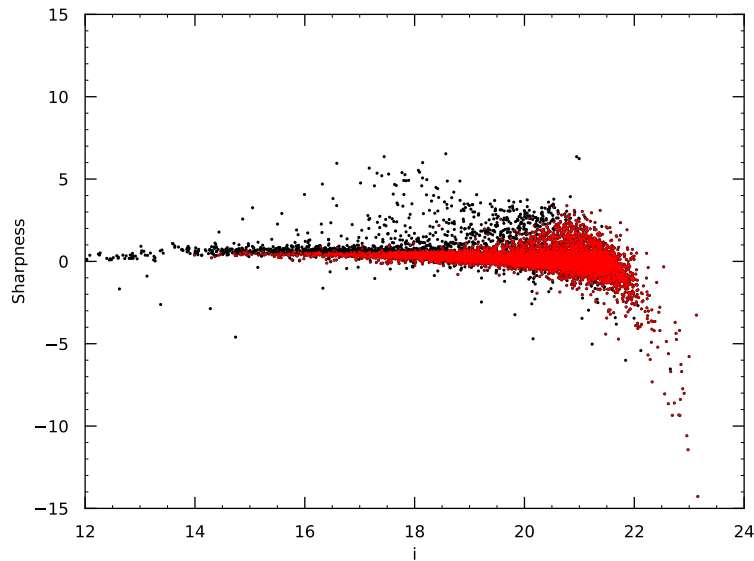


Figure 3: The sharpness values versus  $i$  – band magnitude for stars in one of the individual frames before (black dots) and after applying (red dots) a selection on the  $\chi$  values.

## 4 Quality assurance

The cross-match identification was performed between our final catalogue and *Pan-STARRS* (The *Pan-STARRS* release 1 (PS1) survey-DR1) [8] catalogue with a cross match between the celestial positions and magnitudes to estimate the accuracy of our calibration method. The matches were obtained by search radii in 0.1" to 10" iteratively to check the accuracy of the calibration. Fig. 5 shows the satisfactory of cross-matching result within the desired range of magnitude ( $18 \leq i \leq 22 \text{ mag}$ ).

The completeness limit of our final catalogue has been estimated to determine the accuracy of our photometry. ADDSTAR routine was used to add 3000 artificial stars. These stars were placed randomly on the two of the individual frames in both  $i$ - and  $V$  – band in each of ten trials in 1.0 mag bins starting from  $i = 17 \text{ mag}$  until 26 mag and as the same for the  $V$  – band frame. Then, photometry was applied to the new images in both of  $i$ - and  $V$  – band and the star-finding efficiency and the photometric accuracy were estimated by comparing the output data for these stars to what was put in. Due to the crowdedness of the field, the artificial stars were added in ten individual steps to the frames. Fig. 6 shows that our catalogue is perfectly complete down to  $i = 21 \text{ mag}$ , falling to 80 per cent at  $i = 22.5 \text{ mag}$  and dropping to less than 50 per cent at  $i \sim 23.07 \text{ mag}$ . As can be seen, the  $V$  – band output satisfies the similar completeness levels approximately at the fainter magnitudes ( $V \sim 23.66 \text{ mag}$ ). Generally, we can conclude that the photometry is more than 85 per cent complete at the tip of the red giant branch (RGB-tip), which is obtained 21.9 mag in  $i$  – band. This photometric depth ensures that the thermally pulsing AGBs, are detected in this galaxy. Moreover, the maximum per cent of recovery for stars with magnitudes brighter than 22 mag is significantly more than fainter one. The accuracy of our photometry has been tested and shown in Fig. 7. As can be seen, the difference between the artificial stars magnitudes and the recovered ones ( $\Delta i$ ) is very small until  $i \sim 22 \text{ mag}$  and increases for fainter magnitudes. Thereupon, our photometry is sufficiently complete

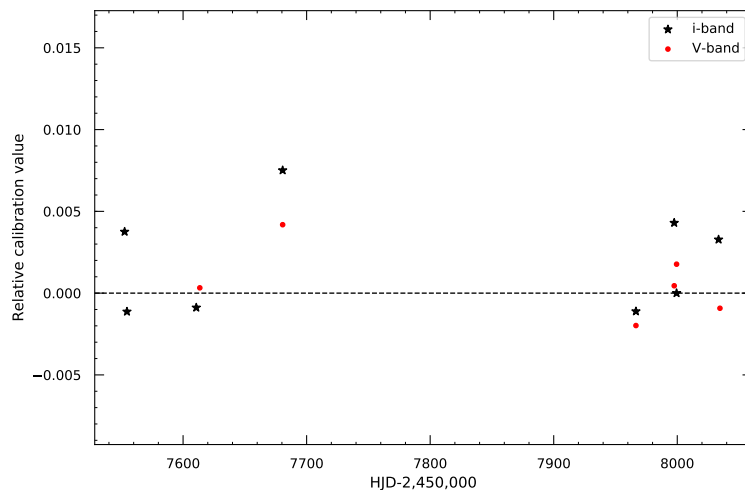


Figure 4: Relative calibration corrections for all of the individual images, as a function of time.

for study the AGBs with the magnitudes lower than  $22 \text{ mag}$  in the  $i$  –  $band$ .

The accuracy of our photometry versus distance from the centre of IC 10, has also been tested by adding 1500 artificial stars to one of the individual images using ADDSTAR routine. The stars have been located randomly with adding the Poisson noise to the image for the magnitudes of  $i = 18, 19 \text{ \& } 20 \text{ mag}$ . At the top and middle panels in Fig. 8, the differences between the artificial input magnitude and the recovered one is very small,  $-\Delta(i) < 0.1 \text{ mag}$ . The stars which are close to the centre of IC 10,  $r < 50 \text{ arcsec}$ , have the differences up to  $-\Delta(i) < 0.7 \text{ mag}$ . As can be seen, the recovered stars are brighter than the input stars which are related to the blending occurred due to crowdedness in the centre of IC 10. At  $i = 20 \text{ mag}$ , the recovered stars regardless of the distance from the centre, are brighter than the input stars and the crowdedness is notable. We conclude that our photometry is accurate enough to the aim of our project of studying the AGBs and RSGs, which they have  $i < 22 \text{ mag}$ .

## 5 Discussion

We identified the stellar population in the central regions of IC 10. The photometry has been carried out within the area of  $0.07 \text{ deg}^2$  ( $13.5 \text{ kpc}^2$ ), the area of CCD4 of WFC. Fig. 9 shows magnitude error versus magnitude for stars in our catalogue in both filters. Vertical lines in red are error bars at each magnitude bins. The magnitude errors at the brighter stars are significantly lower than the stars with the magnitudes more than RGB-tip. Fig. 10 shows the logarithmic distribution of the magnitudes in  $i$ – and  $V$  –  $band$ . The completeness limits are shown for  $i$ – and  $V$  –  $band$  magnitude with green and pink vertical dashed lines, respectively.

We characterize the stellar population in the central regions of IC 10 using the colour-magnitude diagram (CMD) with isochrones calculated by Marigo et al. [39](Fig. 11). The isochrones were calculated for the constant metallicity of  $[Fe/H] = -1.28 \text{ dex}$  [59]. The extinction ( $A_V$ ) of  $1.8 \text{ mag}$  has been obtained which is a best-fit value for our catalogue. Britavskiy et al. changed the extinction coefficient in a range from 0.1 to  $4 \text{ mag}$  with a step

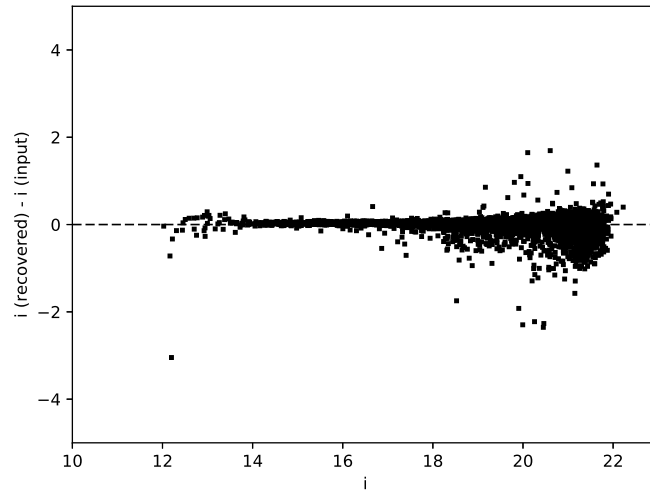


Figure 5: Magnitude differences between INT catalogue and *Pan-STARRS* of IC 10 dwarf galaxy, plotted versus  $i$  – band magnitude for our catalogue

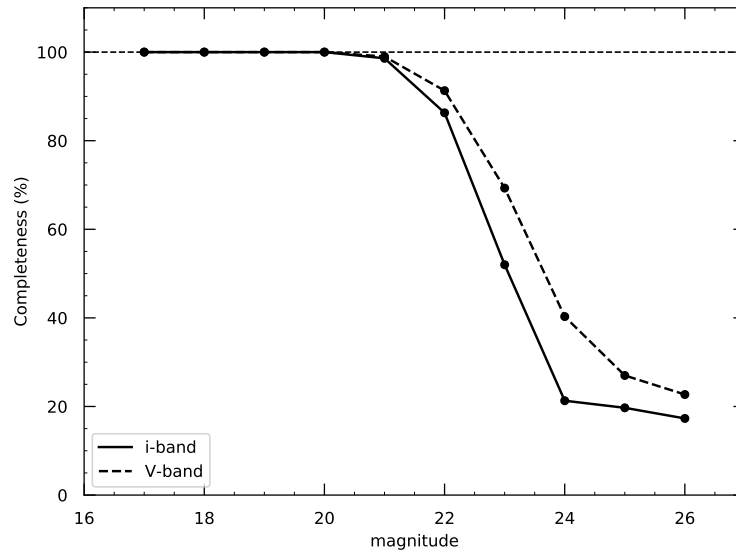


Figure 6: Completeness as a function of  $i$  – band (solid line) and  $V$  – band (dashed line) magnitude.

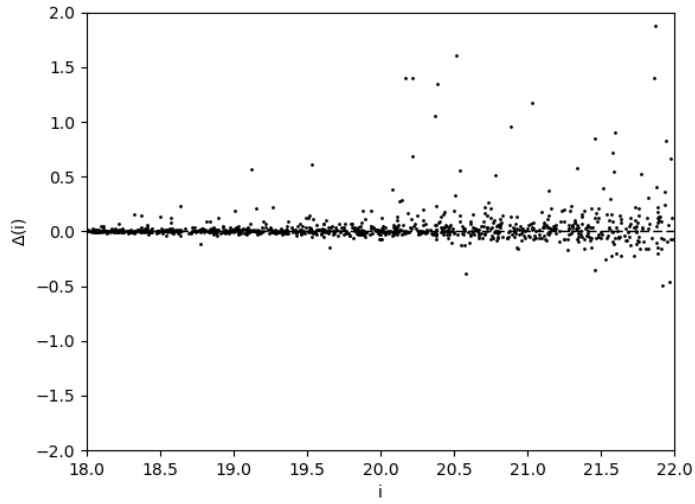


Figure 7: The magnitude difference between the artificial stars magnitudes and the recovered ones versus  $i$ -band magnitude.

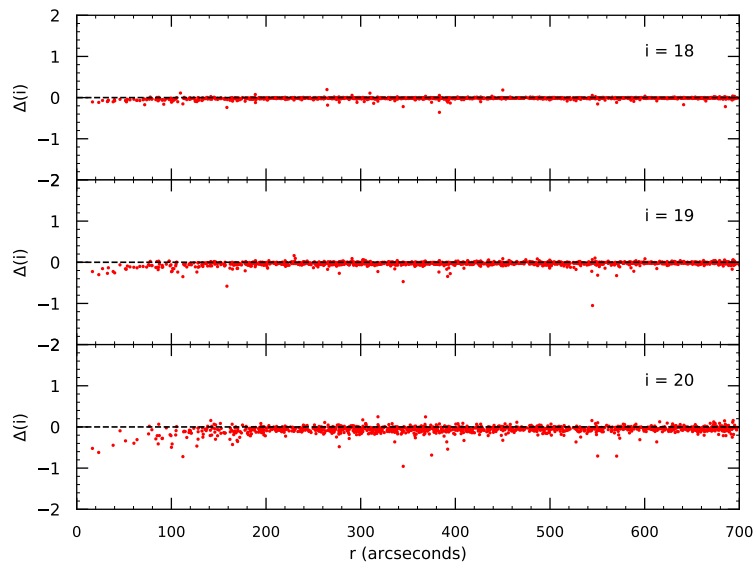


Figure 8: Difference between the input magnitude and recovered magnitude (from an  $i$ -band image) versus distance from the centre of IC 10, for three values of the input magnitude.

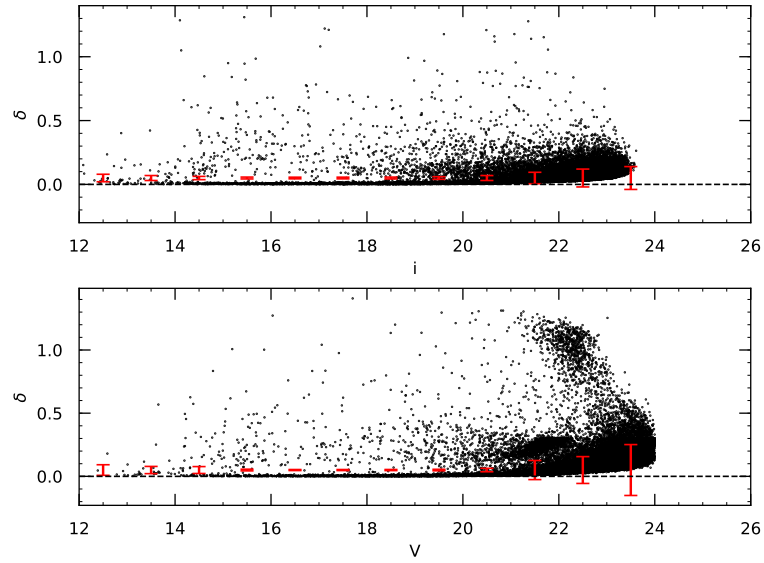


Figure 9: Magnitude error versus magnitude for stars in our catalogue in both of  $i$ - and  $V$ -band. Vertical lines in red are error bars at each magnitude bins.

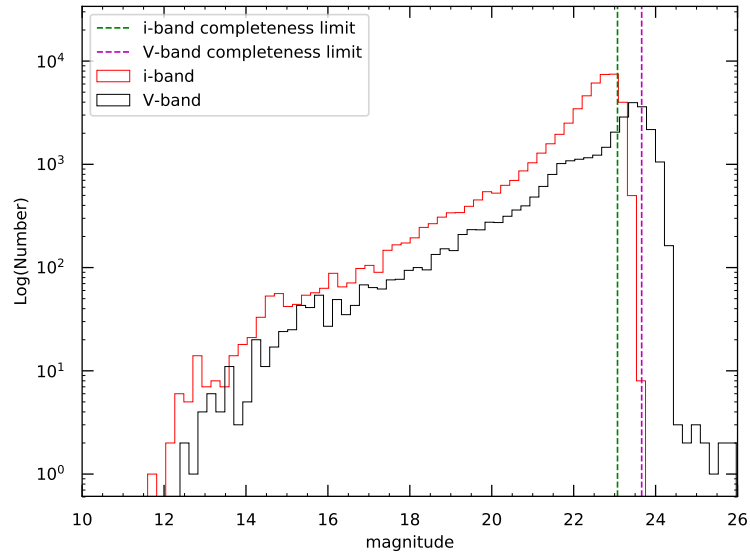


Figure 10: Log number of stars versus magnitude distribution of stars in each photometric band ( $i$ - and  $V$ -band). The completeness level of each band has been inferred and is discussed in the text Sect. 4

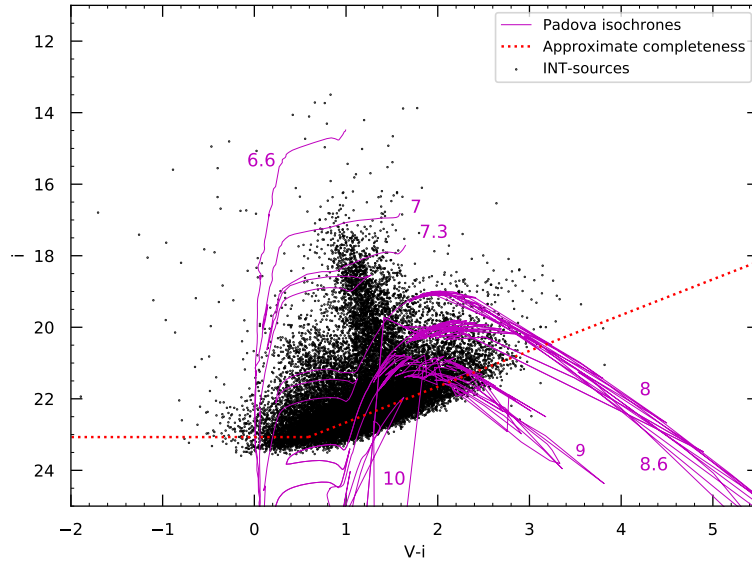


Figure 11: Colour-magnitude diagram of  $i$  vs.  $(V - i)$ . Overplotted are isochrones from Marigo et al. [39] for the constant metallicity of  $[Fe/H] = -1.28 dex$  and a distance modulus of  $24.27 \pm 0.18 mag$ .

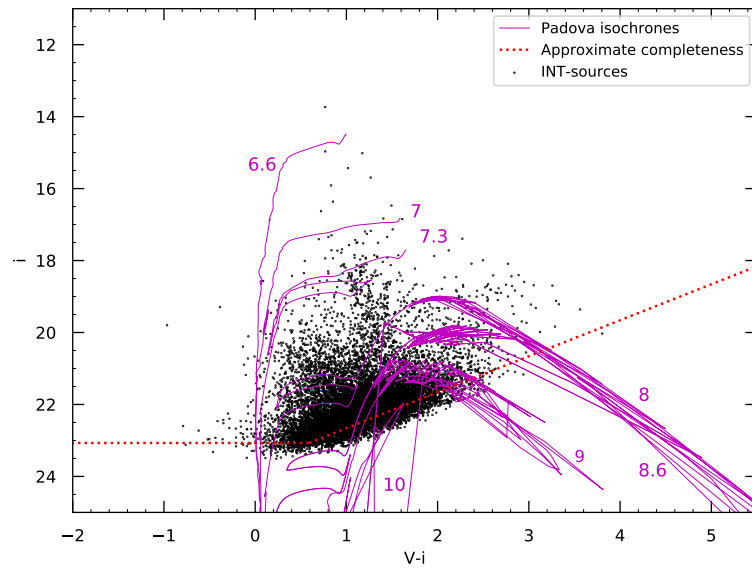


Figure 12: Colour-magnitude diagram of  $i$  vs.  $(V - i)$  for stars in half-light radius of IC 10. Overplotted are isochrones from Marigo et al. [39] for the constant metallicity of  $[Fe/H] = -1.28 dex$  and a distance modulus of  $24.27 \pm 0.18 mag$ .

of 0.1 *mag* for IC 10 [6]. We used their extinction coefficient range to determine the best value that fits to our data well. We obtained the extinction coefficient value in *V* – band of 1.8 *mag* using the report of Britavskiy et al. [6]. The adopted distance modulus of  $\mu = (24.27 \pm 0.18 \text{ mag})$  appears to be appropriate as it fits well on the stellar abundant. Fig. 12 shows the colour-magnitude diagram of *i* versus (*V* – *i*) for half-light radius of IC 10. The isochrones are plotted as described in Fig. 11. Foreground stars have been removed from the stellar population based on the mentioned criterion which is applied on the stars.

IC 10 dwarf galaxy is close to the galactic plane of the Milky Way; therefore, observations suffer from heavy foreground contamination. The level of contamination was explored by detection of stars at Milky Way in the direction of IC 10. This task is performed by calculating the cross-match identification of our catalogue with the Gaia DR2 catalogue [1]. Gaia DR2 contains celestial positions and apparent magnitude in *G* – band for approximately 1.7 billion sources. The photometry in Gaia DR2 consists of three broad bands: a *G* magnitude for all sources and a *G<sub>BP</sub>* and *G<sub>RP</sub>* magnitude for the large majority [1]. Parallaxes (Pa) and proper motions (pm) are available for 1.3 billion of stars at Gaia DR2 catalogue. The cross-match identification between our catalogue and Gaia DR2 is led to obtaining 4488 stars in common between two catalogues. Then, we estimated the distance of common stars at our catalogue based on their parallax values. The stars have been classified to two categories: The stars with the parallax values ( $Pa \geq 0.01 \text{ mas}$ ), which stand for the stars with the distances less than 100 kpc and the stars with the parallax values ( $Pa \leq 0.01 \text{ mas}$ ), which stand for the stars with the distances larger than 100 kpc which they are not considered as the stars at Milky Way. We determined the threshold for the value of  $\frac{Pa}{ePa}$ , which (*ePa*) is the estimated error to parallax measurements for each star to obtain more accurate identifications of the Milky Way stars as the foregrounds. A star is classified as foregrounds if it satisfies either  $Pa/ePa \geq 2 \sigma$  criteria or its proper motion (pm) is more than 0.28 mas/yr in both directions of *RA* and *DEC* [46]. Therefore, we removed them from our final catalogue.

We identified 10800 AGBs based on the number of stars between RGB-tip (21.9 *mag*) and AGB-tip (18.9 *mag*) magnitude. The stars with the low- to medium mass of 0.8-8  $M_{\odot}$  in the final stage of their evolution enter the AGB phase while the stars with the mass of  $M > 8 M_{\odot}$  (massive stars) enter the RSG phase [35, 36, 43]. RSGs are found all the way until the earliest age ( $t \sim 10 \text{ Myr}$ ) which is defined as highest birth mass [23, 27] among these populations. The stellar populations of massive stars, AGBs and RGBs have been shown by the grey lines in the colour-magnitude diagram of our catalogue in Fig. 13. Our catalogue reaches the completeness limit of more than 90 per cent above the RGB-tip around  $i \sim 21.9 \text{ mag}$ . Saturated stars and the stars which are located near the edge of images have been removed from our catalogue and foreground stars are also shown with red dots. The stellar populations of massive, AGB and RGB have been determined by the grey lines in the figure (Fig. 13). According to our results, we will identify the LPVs in IC 10 at our next work to describe the star formation history and chemical enrichment of IC 10 dwarf galaxy. We classified the stars in our catalogue into three populations; massive stars, AGBs and RGBs based on the *i* – band magnitude and (*V* – *i*) colour criteria. As it has been shown in Fig. 13, hot massive stars and cooler ones are separated by the line from (*V* – *i*, *i*) = (0.21, 21.9) *mag* to (*V* – *i*, *i*) = (0.47, 18.9) *mag*, which the massive stars are characterized with the colour bluer than this criteria down to 23.07 *mag* or those have  $i < 18.9 \text{ mag}$ . AGBs and RGBs have the colour redder than these criteria with the magnitude of  $18.9 \text{ mag} < i < 21.9 \text{ mag}$  and  $21.9 \text{ mag} < i < 23.07 \text{ mag}$ , respectively.

Fig. 14 shows the radial distribution of AGBs, RSGs and massive stars within the area of 0.07 deg<sup>2</sup> (13.5 kpc<sup>2</sup>) from the centre of IC 10. As can be seen, most of the stellar populations are located at the centre of the galaxy where their distances are lower than 200 arcsec.

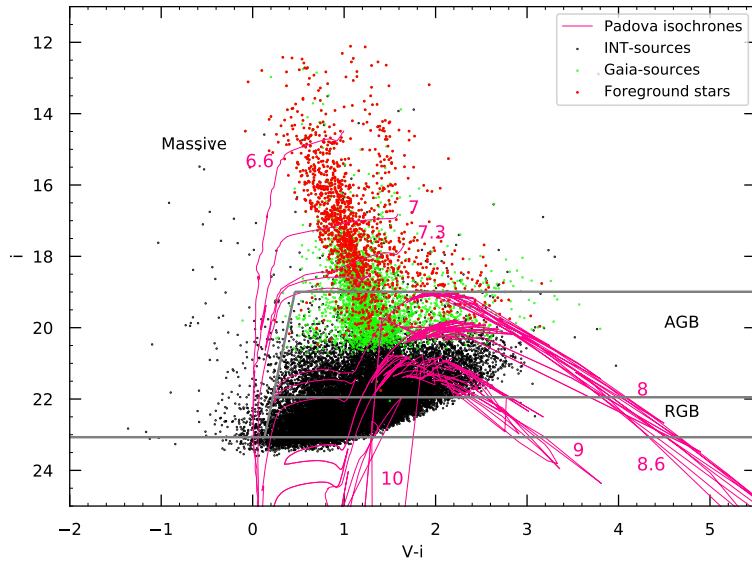


Figure 13: Colour-magnitude diagram of our INT catalogue; Gaia stars and foreground stars are plotted in green and red, respectively. Overplotted are isochrones from Marigo et al. [39], labelled by their logarithmic ages. The grey lines indicate the populations of massive stars, AGBs and RGBs.

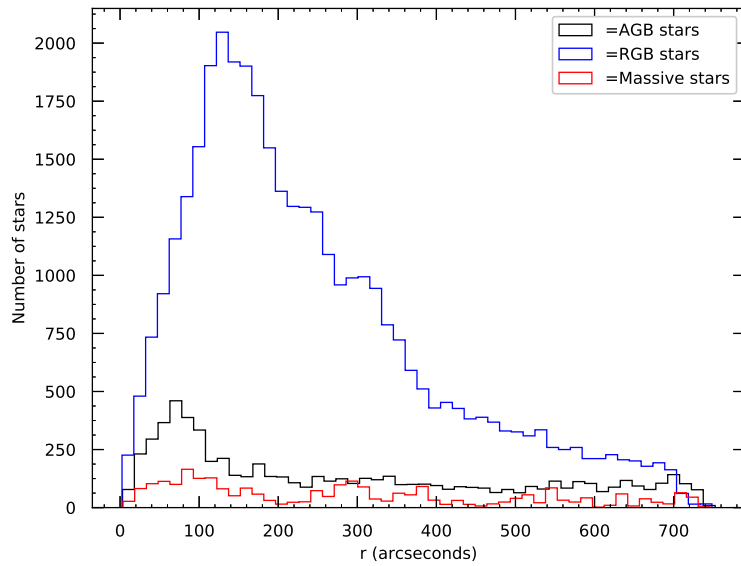


Figure 14: Radial distributions of massive stars (in red), AGBs (in black) and RGBs (in blue) in the image plane within the area of  $0.07 \text{ deg}^2$  from the centre of IC 10.

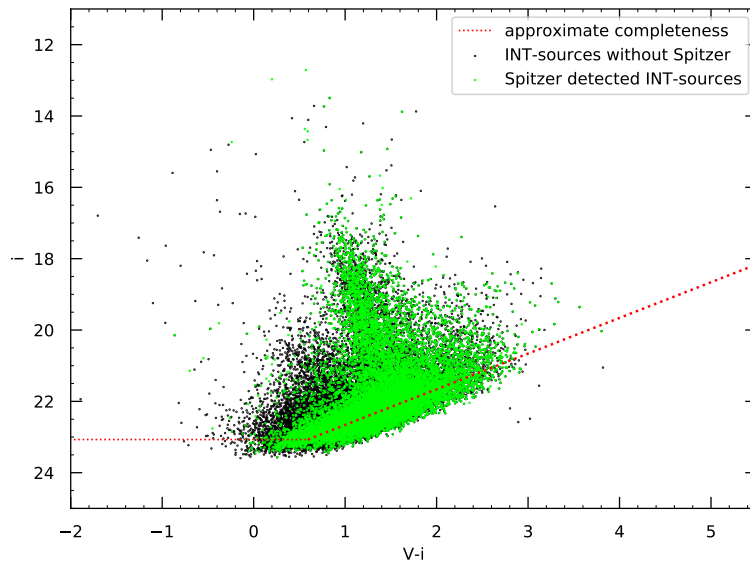


Figure 15: Colour-magnitude diagram of  $i$  vs.  $(V - i)$ . The *Spitzer* detected INT sources are highlighted in green and foregrounds have been removed from the catalogue.

The AGB, RGB and massive populations show some central condensation. The RGBs population has the largest effective radius and the AGBs population has the smallest effective radius among the three populations and AGBs are more centrally concentrated than the RGBs and massive stars.

## 5.1 Cross-identifications in other catalogues

The cross-correlation of our INT-sources with the mid-IR catalogue from the *Spitzer Space Telescope* [4] has been performed and shown in Fig. 15. We obtained the matched stars by search iterations using growing search radii, in steps of  $0.1''$  out to  $1''$  [22]. Boyer et al. [4] performed two epochs of *Spitzer Space Telescope* observations of 50 dwarf galaxies within 1.5 Mpc that is used to identify dust-producing AGBs and massive stars. They described DUSTiNGS (DUST in Nearby Galaxies with *Spitzer*) which is a 3.6 and  $4.5 \mu\text{m}$  post-cryogen *Spitzer Space Telescope* imaging survey of 50 dwarf galaxies within 1.5 Mpc that is created to identify dust-produced AGBs and massive stars (DUSTiNGS I) [4]. The 60975 sources of the good source catalogue in DUSTiNGS I project, are covered by our INT-data in the same area. Among these, 28490 are in our photometric catalogue; about 27 per cent of them are fainter than the RGB-tip magnitude. We did not recover the 32485 *Spitzer* sources because of being located at the edges of the frames or being very faint in the optical observation at our data. Therefore, the recovery rate is about 47 per cent.

Boyer et al. in DUSTiNGS IV project reported the near-IR *Hubble Space Telescope* (*HST*) observations of six star-forming DUSTiNGS galaxies using medium-band filters on *HST*'s WFC3/IR to identify AGB spectral types. They combined their observations with mid-IR data from *Spitzer* and distinguished the C-type (Carbon-rich) and M-type (Oxygen-rich) of dust-producing stars by their atmospheric chemistry and they showed that dust can form even in very metal-poor systems ( $Z \sim 0.008 Z_{\odot}$ ) [5]. The C- and M-type stars are identified by photometric surveys using broadband near-IR (JHK) or narrow-band optical filters [5].

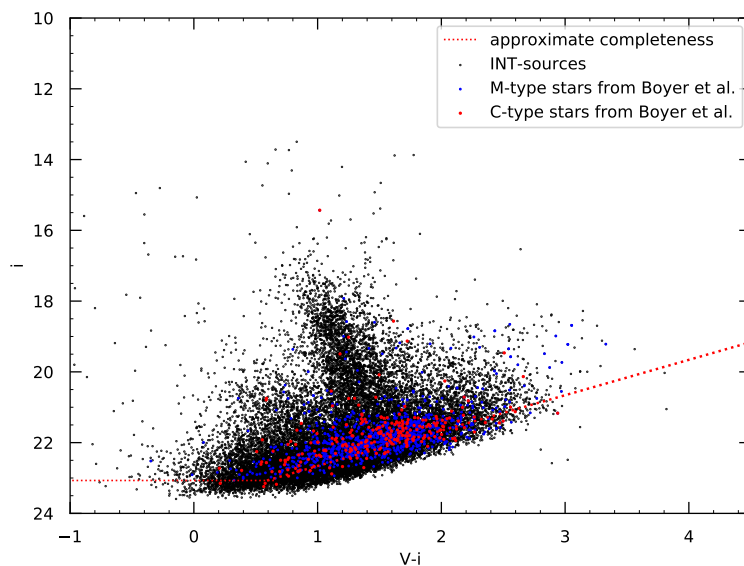


Figure 16: colour-magnitude diagram of  $i$  vs.  $(V - i)$  shows the M-type and C-type stars from the Boyer et al. that were detected in our INT survey.

VO, TiO, and  $H_2O$  molecular structures affect the broadband near-IR filters in M-type stars and also CN and  $C_2$  molecular structures affect the broadband near-IR in C-type stars. However, the narrow-band filters are influenced by TiO and CN molecular structures at  $\lambda < 7000 \text{ \AA}$  [5]. We also performed cross-match identification between AGBs in our catalogue and AGBs catalogue of Boyer et al. in DUSTiNGS IV project [5]. The number of 2368 AGBs (out of 2896 AGBs in the *Spitzer* and *Hubble Space Telescope (HST)* catalogue in the same area) in the DUSTiNGS IV project is recovered by us. The recovery rate has been estimated at 82 per cent level. The photometry in optical wavebands is not deep enough to recover all of the AGBs in our catalogue. On the other hand, very dusty AGBs can not be detected at our optical photometry because very dusty AGBs are very faint in the optical wavebands. We identified the C- and M-type stars using the matched stars between our catalogue and the *HST* catalogue in the number of 441 and 1927 stars, respectively; The C- and M-type stars are highlighted at the colour-magnitude diagram of  $i$  vs.  $(V - i)$  in red and blue dots, respectively (Fig. 16).

## 6 Conclusion

We used the INT optical monitoring survey of IC 10 dwarf galaxy in the Local Group in the  $i$ - and  $V$ -band filters. A photometry catalogue was obtained with the 48578 stars within the area of  $0.07 \text{ deg}^2$  ( $13.5 \text{ kpc}^2$ ) of which 10800 stars are AGBs. Cross-match identification for our catalogue has been obtained by *Pan-STARRS* catalogue, *Spitzer Space Telescope* mid-IR catalogue and *HST* catalogue. We found that the RGBs population has the largest effective radius among the three populations (AGBs, RGBs, and massive stars), while the AGBs population has the smallest effective radius in the IC 10 image plane. The number of 2368 AGBs in the *Spitzer* catalogue were recovered by our INT catalogue with the recovery rate of 82 per cent. The number of 441 and 1927 stars in *HST* catalogue have been identified as C-type and M-type stars, respectively which recovered by our INT catalogue. In the next

paper in these series, we will identify Long-Period variable stars (LPVs) to explain the star formation history and dust production in the IC 10 dwarf irregular galaxy.

## Acknowledgement

The observing time for this survey is provided by the Iranian National Observatory and the UK-PATT allocation of time to programmes *I/2016B/09* and *I/2017B/04* (PI: J. van Loon). The authors thank the Iranian National Observatory and the School of Astronomy (IPM) for the financial support of this project. We thank Atefeh Javadi and Jacco Th. van Loon for their valuable comments and great help during this project. We thank the ING observers for service mode observations. Also, we thank Habib Khosroshahi, Elham Saremi, Alireza Molaeinezhad, Arash Danesh, James Bamber, Iain McDonald, Mojtaba Raouf, Philip Short, Lucia Surez-Andrs, Rosa Clavero and Ghassem Gozaliasl for their efforts during the observations. We are grateful to Peter Stetson for sharing his photometry routines and his valuable comments and we also thank the anonymous referee for her/his suggestions that helped improve the manuscript.

## References

- [1] Arenou, F., Luri, X., Babusiaux, C., Fabricius, C., Helmi, A., Muraveva, T., & et al. 2018, *A&A*, 616, A17
- [2] Ashley, T., Elmegreen, B. G., Johnson, M., Nidever, D. L., & et al. 2014, *AJ*, 148, 130
- [3] Borissova, J., Georgiev, L., Rosado, M., & et al. 2000, *A&A*, 363, 130
- [4] Boyer, M. L., McQuinn, K. B. W., Barmby, P., & et al. 2015, *ApJ*, 800, 51
- [5] Boyer, M. L., & et al. 2017, *ApJ*, 851, 152
- [6] Britavskiy, N. E., Bonanos, A. Z., Herrero, A., & et al. 2019, *A&A*, 631, 18
- [7] Brunthaler, A., Reid, M. J., Falcke, H., Henkel, C., Menten, K. M. 2007, *A&A*, 462, 101
- [8] Chambers, K. C., Magnier, E. A., Metcalfe, N., & et al. 2016, <https://ui.adsabs.harvard.edu/abs/2016arXiv161205560C>
- [9] Crowther, P. A., Drissen, L., Abbott, J. B., Royer, P., & Smartt, S. J. 2003, *A&A*, 404, 483
- [10] Dell’Agli, F., & et al. 2018, *MNRAS*, 479, 5035
- [11] Demers, S., Battinelli, P. & Letarte, B. 2004, *A&A*, 424, 125
- [12] Erben, T., & et al. 2005, *AN*, 326, 432
- [13] Garca-Gil, A., Muoz-Tun, C., & Varela, A. M. 2010, *PASP*, 122, 1109
- [14] Gholami, M., Javadi, A., van Loon, J. Th., & et al. 2019, *IAUS*, 344, 70
- [15] Goldman, S. R., & et al. 2019, *ApJ*, 877, 49

- [16] Hamedani Golshan, R., Javadi, A., van Loon, J. Th., Khosroshahi, H., & Saremi, E. 2017, MNRAS, 466, 1764
- [17] Hashemi, S. A., Javadi, A., & van Loon, J. Th. 2019, MNRAS, 483, 4751
- [18] Hashemi, S. A., Javadi, A., & van Loon, J. Th. 2017, MmSAI, 88, 436
- [19] Hashemi, S. A., Javadi, A., & van Loon, J. Th. 2019, IAUS, 344, 77
- [20] Hunter, D. A., & et al. 2012, AJ, 144, 134
- [21] Ita, Y. & Matsunaga, N. 2011, MNRAS, 412, 2345
- [22] Javadi, A., van Loon, J. Th., & Mirtorabi, M. T. 2011, ASPC, 445, 497
- [23] Javadi, A., van Loon, J. Th., & Mirtorabi, M. T. 2011, 414, 3394
- [24] Javadi, A., van Loon, J. Th., Khosroshahi, H., & Mirtorabi, M. T. 2013, MNRAS, 432, 2824
- [25] Javadi, A., & et al. 2015, MNRAS, 447, 3973
- [26] Javadi, A., van Loon, J. Th., & Khosroshahi, H. 2015, PKAS, 30, 355
- [27] Javadi, A., van Loon, J. Th., & Khosroshahi, H. 2016, MmSAI, 87, 278
- [28] Javadi, A., van Loon, J. Th., Khosroshahi, H., Tabatabaei, F., Hamedani Golshan, R., & Rashidi, M. 2017, MNRAS, 464, 2103
- [29] Javadi, A., & van Loon, J. Th. 2017, JPhCS, 869a2062
- [30] Javadi, A., & van Loon, J. Th. 2018, IAUS, 343, 283
- [31] Jordi, K., Grebel, E. K., & Ammon, K. 2006, A&A, 460, 339
- [32] Karachentsev, L. D., Tikhonov, N. A. 1993, A&A, 100, 227
- [33] Kim, M., Kim, E., Hwang, N., & et al. 2009, ApJ, 703, 816
- [34] Leroy, A., Bolatto, A., Walter, F., & Blitz, L. 2006, AJ, 643, 825
- [35] Levesque, E. M., Massey, P., Olsen, K. A. G., Plez, B., Josselin, E., & et al. 2005, ApJ, 628, 973
- [36] Levesque, E. M., Leitherer, C., Bennett, P., Morris, P., & van Loon, J. Th. 2010, ASP Conf., 425, 103
- [37] Lim, S. & Lee, M. G. 2015, ApJ, 804, 123
- [38] van Loon, J. Th., Groenewegen, M. A. T., de Koter, A., & et al. 1999, A&A, 351, 559
- [39] Marigo, P., Girardi, L., Bressan, A., & et al. 2017, ApJ, 835, 77
- [40] Massey, P. & Armandroff, T. E. 1995, AJ, 109, 2470
- [41] McConnachie, A. W. 2012, AJ, 144, 4
- [42] McQuinn, K. B. W., Skillman, E. D., Dolphin, A. E., Berg, D. & Kennicutt, R. 2016, ApJ, 826, 21

- [43] Meynet, G., & et al. 2014, *A&A*, 575, A60
- [44] Rezaeikh, S., Javadi, A., Khosroshahi, H., & van Loon, J. Th. 2014, *MNRAS*, 445, 2214
- [45] Roberts, M. S. 1962, *AJ*, 67, 431
- [46] Roeland, P. van der Marel, & et al. 2019, *AJ*, 872, 24
- [47] Sanna, N., Bono, G., Monelli, M., & et al. 2008, *Mem. Soc. Astron. Ital.*, 79, 747
- [48] Sanna, N., Bono, G., Stetson, P. B., & et al. 2009, *ApJ*, 699, L84
- [49] Saremi, E., Javadi, A., van Loon, J. Th., & et al. 2017, *J. Phys. Conf. Ser.*, 869, 012068
- [50] Saremi, E., Abedi, A., Javadi, A., van Loon, J. Th., & khosroshahi, H. 2017, *IJAA*, 4, 19
- [51] Saremi, E., Javadi, A., van Loon, J. Th., Khosroshahi, H., & Toriki, M. 2019, *IAUS*, 339, 336
- [52] Saremi, E., Javadi, A., van Loon, J. Th., Khosroshahi, H., & et al. 2019, *IAUS*, 344, 125
- [53] Sloan, G. C., Matsuura, M., Lagadec, E., & et al. 2012, *ApJ*, 752, 140
- [54] Sloan, G. C., Kraemer, K. E., McDonald, I., & et al. 2016, *ApJ*, 826, 44
- [55] Stetson, P. B. 1987, *PASP*, 99, 191
- [56] Stetson, P. B. 1990, *ASPC*, 102, 932
- [57] Stetson, P. B. 1994, *PASP*, 106, 250
- [58] Tehrani, K., Crowther, P. A., & Archer, I. 2017, *MNRAS*, 472, 4618
- [59] Tikhonov, N. A., & Galazutdinova, O. A. 2010, *Astronomy Lett.*, 35, 11, 748
- [60] van Loon, J. Th., Cohen, M., Oliveira, J. M., & et al. 2008, *A&A*, 487, 1055
- [61] Whitelock, P. A., Feast, M. W., & Pottasch, S. R. 1987, *Ap&SSL*, 132, 269
- [62] Wilcots, E. M., & Miller, B. W. 1998, *AJ*, 116, 2363
- [63] Yuan, et al. 2018, *AJ*, 156, 112